NUMERICAL SIMULATION OF HIGH- SPEED FLOWS WITH SHOCK WAVE TURBULENT BOUNDARY LAYER INTERACTIONS

S. Y. Moon and C. H. Sohn

충격파와 난류경계층의 상호작용에 대한 수치해석

문 수 연, 손창현

The Interactions of shock wave with turbulent boundary layers in high-speed flows cause complex flowfields which result in increased adverse pressure gradients, skin friction and temperature. Accurate and reliable prediction of such phenomena is needed in designing high-speed propulsion systems. Such analyses of the complex flowfelds require sophisticated numerical scheme that can resolve interactions between shock wave and boundary layers accurately. Therefore the purpose of the present article is to introduce an accurate and efficient mixed explicit-implicit generalized Galerkin finite element method. To demonstrate the validity of the theory and numerical procedure, several benchmark cases are investigated.

Key Words: Finite element method, shock wave, boundary layer, interactions, computational fluid dynamics(CFD),Mixed explicit-implicit method

1. Introduction

The nature of high speed flows gives rise to unavoidable interactions between shock wave and boundary layers which bring about serious problems in flight performance. Flow separations caused by the interactions not only increase drag and heating rate but also cause the unstart condition near throats of inlets. Peak values of skin friction, surface pressure and heat transfer observed near the reattachment points of the separated flow are essential in establishing the limits of mean thermal loads on high speed aerospace vehicles. Moreover, the unsteady characteristics of turbulence appear as serious additional thermal loads on such vehicles. Thus, accurate and reliable prediction of such phenomena is needed in designing high-speed propulsion systems.

Chung and his co-workers [1,2] have studied finite element strategies as applied to shock wave turbulent boundary layer interactions. The main emphasis in the present study is to establish the basic theory and computational strategies of the mixed explicit-implicit generalized Galerkin

method(MEI-GGM) and to present preliminary computational results.

2. MEI Formulation

For the general purpose program considering the compressible turbulent flows, we write the conservation form of the Navier-Stokes system of equations as

$$\frac{\partial \mathbf{U}}{\partial t}+\frac{\partial \mathbf{F}_i}{\partial x_i}+\frac{\partial \mathbf{G}_i}{\partial x_i}=\mathbf{B} \qquad (1)$$

where $\mathbf{U}$, $\mathbf{F}_i$, $\mathbf{G}_i$, and $\mathbf{B}$ denote the conservation flow variables, convection flux variables, diffusion flux variables, and source terms, respectively,

$$\mathbf{U}=\begin{bmatrix}\rho\\ \rho v_j\\ \rho E_k\\ \rho K\\ \rho\varepsilon\end{bmatrix} \quad \mathbf{F}_i=\begin{bmatrix}\rho v_i\\ \rho v_i v_j+p\delta_{ij}\\ \rho E v_i+p v_i\\ \rho K v_i\\ \rho\varepsilon v_i\end{bmatrix}$$

$$\mathbf{G}_j=\begin{bmatrix}0\\ -\tau_{ij}\\ -\tau_{ij}v_j+q_i\\ \mu_k K_{,i}\\ \mu_\varepsilon \varepsilon_{,i}\end{bmatrix} \quad \mathbf{B}=\begin{bmatrix}0\\ 0\\ S_e\\ S_k\\ S_e\end{bmatrix}$$

where τ_{ij} denotes the sum of both physical and turbulence shear stresses, K and ε are the turbulent kinetic energy and its dissipation rate, respectively, and **B** contains source terms. The Sutherland temperature-dependent viscosity and thermal conductivity are used in this analysis.

To implement compressibility or dilatational dissipation effects, the turbulent kinetic energy transport equation as proposed by Sarkar[3] will be utilized.

$$\rho\frac{\partial K}{\partial t}+\rho(K\,v_i)_{,i}=-\rho(\varepsilon+\varepsilon_d)+\textit{diffusion terms} \qquad (2)$$

where ε_d is the kinetic energy dissipation rate due to dilatation or compressibility,

$$\varepsilon_d=\xi F(M_t)\varepsilon \qquad (3)$$

where $F(M_t)$ is a prescribed function of the turbulent Mach number M_t. Using the Sarkar model ,

$$M_t^2=\left(\frac{2K}{a^2}\right)^{1/2} \qquad (4)$$

and ξ is a closure coefficient. As proposed by Sarkar we adopt $\xi=1$ and $F(M_t)=M_t^2$.

In expanding $\mathbf{U}^{n+1}$ in Taylor series about $\mathbf{U}^n$, we introduce the implicitness parameters s_1 and s_2 for the first and second derivatives of **U** with respect to time, respectively,

$$\mathbf{U}^{n+1}=\mathbf{U}^n+\Delta t\frac{\partial \mathbf{U}^{n+s_1}}{\partial t}+\frac{\Delta t^2}{2}\frac{\partial^2 \mathbf{U}^{n+s_{21}}}{\partial t^2}+O(\Delta t^3) \qquad (5)$$

$$\frac{\partial \mathbf{U}^{n+s_1}}{\partial t}=\frac{\partial \mathbf{U}^n}{\partial t}+s_1\frac{\partial \Delta\mathbf{U}^{n+1}}{\partial t} \quad 0\le s_1\le 1 \qquad (6a)$$

$$\frac{\partial^2 \mathbf{U}^{n+s_2}}{\partial t^2}=\frac{\partial^2 \mathbf{U}^n}{\partial t^2}+s_2\frac{\partial^2 \Delta\mathbf{U}^{n+1}}{\partial t^2} \quad 0\le s_2\le 1 \qquad (6b)$$

where $\Delta\mathbf{U}^{n+1}=\mathbf{U}^{n+1}-\mathbf{U}^n$.

Substituting Eq. (6) into Eq. (5) yields

$$\Delta \mathbf{U}^{n+1} = \Delta t\left(\frac{\partial \mathbf{U}^n}{\partial t} + s_1 \frac{\partial \Delta \mathbf{U}^{n+1}}{\partial t}\right) + \frac{\Delta t^2}{2}\left(\frac{\partial^2 \mathbf{U}^n}{\partial t^2} + s_2 \frac{\partial^2 \Delta \mathbf{U}^{n+1}}{\partial t^2}\right) + O(\Delta t^3) \qquad (7)$$

$$\frac{\partial \mathbf{U}}{\partial t} = -\frac{\partial \mathbf{F}_i}{\partial x_{i,}} - \frac{\partial \mathbf{G}_i}{\partial x_i} + \mathbf{B} \qquad (8)$$

Here $\mathbf{F}_i$ is a function of $\mathbf{U}$ and $\mathbf{G}_i$ is a function of $\mathbf{U}$ and its gradient $\mathbf{U}_{,k}$ so that we denote the convective Jacobian $\mathbf{a}_i$, dissipative Jacobian $\mathbf{b}_i$, dissipative gradient Jacobian $\mathbf{c}_{ik}$ and the source Jacobian $\mathbf{d}$ as

$$\frac{\partial^2 \mathbf{U}}{\partial t^2} = -\frac{\partial}{\partial x_i}\left(\mathbf{a}_i \frac{\partial \mathbf{U}}{\partial t}\right) - \frac{\partial}{\partial x_i}\left(\mathbf{b}_i \frac{\partial \mathbf{U}}{\partial t}\right) - \frac{\partial^2}{\partial x_i \partial x_j}\left(\mathbf{c}_{ij} \frac{\partial \mathbf{U}}{\partial t}\right) + \mathbf{d}\left(\frac{\partial \mathbf{U}}{\partial t}\right) \qquad (9)$$

$$\mathbf{a}_i = \frac{\partial \mathbf{F}_i}{\partial \mathbf{U}}, \qquad \mathbf{b}_i = \frac{\partial \mathbf{G}_i}{\partial \mathbf{U}}, \qquad \mathbf{c}_{ij} = \frac{\partial \mathbf{G}_i}{\partial \mathbf{U}_{,j}},$$

$$\mathbf{d} = \frac{\partial \mathbf{B}}{\partial \mathbf{U}} \qquad (10)$$

Substituting Eqs. (8), (9) and (10) into Eq. (7) yields

$$\Delta \mathbf{U}^{n+1} = \Delta t\left[-\frac{\partial \mathbf{F}_i^n}{\partial x_i} - \frac{\partial \mathbf{G}_i^n}{\partial x_i} + \mathbf{B}^n\right] + s_1\left(-\frac{\partial \Delta \mathbf{F}_i^{n+1}}{\partial x_i} - \frac{\partial \Delta \mathbf{G}_i^{n+1}}{\partial x_i} + \Delta \mathbf{B}^{n+1}\right) + \frac{\Delta t^2}{2}\left\{\left[\frac{\partial}{\partial x_i}\left(\mathbf{a}_i + \mathbf{b}_i\right)\left(\frac{\partial \mathbf{F}_i^n}{\partial x_i} + \frac{\partial \mathbf{G}_i^n}{\partial x_i} - \mathbf{B}^n\right)\right]\right.$$
$$\left. - \mathbf{d}\left(\frac{\partial \mathbf{F}_i^n}{\partial x_i} + \frac{\partial \mathbf{G}_i^n}{\partial x_i} - \mathbf{B}^n\right)\right\} + s_2\left[\frac{\partial}{\partial x_i}\left(\mathbf{a}_i + \mathbf{b}_i\right)\left(\frac{\partial \Delta \mathbf{F}_j^{n+1}}{\partial x_j} + \frac{\partial \Delta \mathbf{G}_j^{n+1}}{\partial x_j} - \Delta \mathbf{B}^{n+1}\right)\right] \qquad (11)$$

In order to provide different implicitness (different amount of damping or dissipation) to different physical quantities, we reassign s_1 and s_2 associated with $\mathbf{G}_i$, respectively.

$$s_1 \Delta \mathbf{G}_i \Rightarrow s_3 \Delta \mathbf{G}_i \ , \ s_1 \Delta \mathbf{B} \Rightarrow s_5 \Delta \mathbf{B} \qquad (12a)$$

$$s_2 \Delta \mathbf{G}_i \Rightarrow s_4 \Delta \mathbf{G}_i \ , \ s_2 \Delta \mathbf{B} \Rightarrow s_6 \Delta \mathbf{B} \qquad (12b)$$

second order with the various implicitness parameters defined as s_1 = first order convective implicitness parameter, s_2 = second order convective implicitness parameter, s_3 = first order diffusion implicitness parameter, s_4 = diffusion implicitness parameter. s_5 = first order source term implicitness parameter, s_6 = source term parameter. Notice that the idea behind this reassignment of implicitness parameters for the viscous terms is motivated by the need to alleviate stiffness caused by viscous boundary layers, particularly in turbulent flows, and diffusion boundary layers in chemically reacting flows. It can be shown that all currently available schemes (finite differences or finite elements) arise from some combinations of the proposed implicitness parameters.

$$\Delta \mathbf{B} = \frac{\partial \mathbf{B}}{\partial \mathbf{U}} \Delta \mathbf{U}^{n+1} = \mathbf{d} \Delta \mathbf{U}^{n+1} \qquad (13)$$

Substituting Eq. (12) and (13) into Eq. (11) leads to the residual,

$$\Delta\mathbf{U}^{n+1}+\Delta t\left[s_1\left(\frac{\partial \mathbf{a}_i\Delta\mathbf{U}^{n+1}}{\partial x_i}\right)\right.$$

$$\left.+s_3\left(\frac{\partial \mathbf{b}_i\Delta\mathbf{U}^{n+1}}{\partial x_i}+\frac{\partial^2\mathbf{c}_{ij}\Delta\mathbf{U}^{n+1}}{\partial x_i\partial x_j}\right)-s_5\mathbf{d}\Delta\mathbf{U}^{n+1}\right]$$

$$-\frac{\Delta t^2}{2}\left\{s_2\left[\frac{\partial^2\left(\mathbf{a}_i\mathbf{a}_j+\mathbf{b}_i\mathbf{a}_j\right)\Delta\mathbf{U}^{n+1}}{\partial x_i\partial x_j}-\mathbf{d}\frac{\partial \mathbf{a}_i\Delta\mathbf{U}^{n+1}}{\partial x_i}\right]\right.$$

$$+s_4\left[\left(\frac{\partial^2\left(\mathbf{a}_i\mathbf{b}_j+\mathbf{b}_i\mathbf{b}_j\right)\Delta\mathbf{U}^{n+1}}{\partial x_i\partial x_j}\right)\right.$$

$$\left.\left.-\mathbf{d}\left(\frac{\partial \mathbf{b}_i\Delta\mathbf{U}^{n+1}}{\partial x_i}+\frac{\partial^2\mathbf{c}_{ij}\Delta\mathbf{U}^{n+1}}{\partial x_i\partial x_j}\right)\right]\right.$$

$$\left.-s_6\left[\frac{\partial\left(\mathbf{a}_i+\mathbf{b}_i\right)\Delta\mathbf{U}^{n+1}}{\partial x_i}-\mathbf{d}\Delta\mathbf{U}^{n+1}\right]\right\}$$

$$+\Delta t\left(\frac{\partial \mathbf{F}_i^n}{\partial x_i}+\frac{\partial \mathbf{G}_i^n}{\partial x_i}-\mathbf{B}^n\right)$$

$$-\frac{\Delta t^2}{2}\left[\frac{\partial}{\partial x_i}\left(\mathbf{a}_i+\mathbf{b}_i\right)\left(\frac{\partial \mathbf{F}_j^n}{\partial x_j}+\frac{\partial \mathbf{G}_j^n}{\partial x_j}-\mathbf{B}^n\right)\right.$$

$$\left.-\mathbf{d}\left(\frac{\partial \mathbf{F}_i^n}{\partial x_i}+\frac{\partial \mathbf{G}_i^n}{\partial x_i}-\mathbf{B}^n\right)\right]+O\left(\Delta t^3\right)=0 \quad (14)$$

Eq.(14) can be rearranged as follows

$$\mathbf{R}=\mathbf{A}\Delta\mathbf{U}^{n+1}+\frac{\partial\left(\mathbf{E}_i\Delta\mathbf{U}^{n+1}\right)}{\partial x_i}+\frac{\partial^2\left(E_{ij}\Delta\mathbf{U}^{n+1}\right)}{\partial x_i\partial x_j}$$

$$+\mathbf{Q}^n+O(\Delta t^3) \quad (15)$$

where all Jacobians $\mathbf{a}_i$, $\mathbf{b}_i$, $\mathbf{c}_{ij}$, and $\mathbf{d}$ are assumed to remain constant spatially within each time step and to be updated at subsequent time steps.

The Galerkin finite element analysis of Eq. (15) may now be carried out as follows:

$$\left(\mathbf{A}+\frac{\partial}{\partial x_i}\mathbf{E}_i+\frac{\partial^2}{\partial x_i\partial x_j}\mathbf{E}_{ij}\right)\Delta\mathbf{U}^{n+1}=-\mathbf{Q}^n \quad (16)$$

$$\mathbf{A}=\mathbf{I}-\Delta t s_5\mathbf{d}-\frac{\Delta t^2}{2}s_6\mathbf{d} \quad (17)$$

$$\mathbf{E}_i=\Delta t\left(s_1\mathbf{a}_i+s_3\mathbf{b}_i\right)+\frac{\Delta t^2}{2}\left[s_6\mathbf{d}\left(\mathbf{a}_i+\mathbf{b}_i\right)\right.$$

$$\left.+s_2\mathbf{d}\mathbf{a}_i+s_4\mathbf{d}\mathbf{b}_i\right] \quad (18)$$

$$\mathbf{E}_{ij}=\Delta t s_3\mathbf{c}_{ij}-\frac{\Delta t^2}{2}\left[s_2\left(\mathbf{a}_i\mathbf{a}_j+\mathbf{b}_i\mathbf{a}_j\right)\right.$$

$$\left.+s_4\left(\mathbf{a}_i\mathbf{b}_j+\mathbf{b}_i\mathbf{b}_j-\mathbf{d}\mathbf{c}_{ij}\right)\right] \quad (19)$$

$$\mathbf{Q}^n=\frac{\partial}{\partial x_i}\left[\left(\Delta t+\frac{\Delta t^2}{2}\mathbf{d}\right)\left(\mathbf{F}_i^n+\mathbf{G}_i^n\right)\right.$$

$$\left.+\frac{\Delta t^2}{2}\left(\mathbf{a}_i+\mathbf{b}_i\right)\mathbf{B}^n\right]$$

$$-\frac{\partial^2}{\partial x_i\partial x_j}\left[\frac{\Delta t^2}{2}\left(\mathbf{a}_i+\mathbf{b}_i\right)\left(\mathbf{F}_j^n+\mathbf{G}_j^n\right)\right]$$

$$-\left(\Delta t+\frac{\Delta t^2}{2}\mathbf{d}\right)\mathbf{B}^n \quad (20)$$

Applications to the finite element method are formulated in [4]

3. Results and Discussions

A typical benchmark problem for the two-dimensional compressible laminar flow is a classical flat problem. The problem have been solved by several workers as it can be regarded as a first step in the process of solving viscous

supersonic flow.

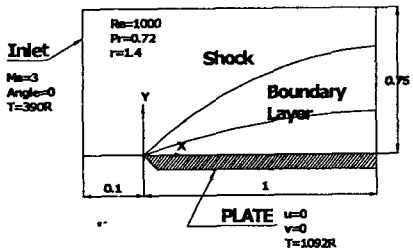

Fig. 1 Geometry and boundary conditions of a flat plate problem.

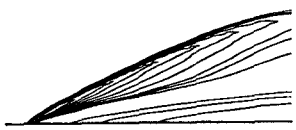

Fig.2. Density contours(Max=1.97294 Min=0.4164)

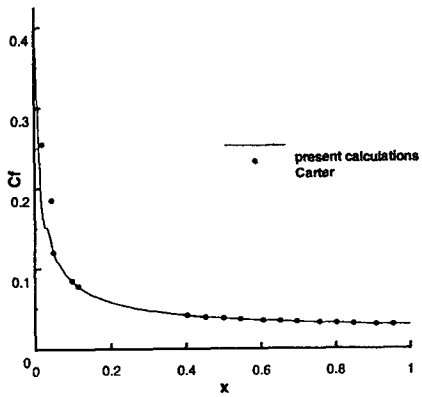

Fig.3 Comparison of skin friction distribution

Fig. 1 shows the geometry and boundary conditions of the flat plate. The flow variables at the upstream entrance boundary are held as shown in Fig. 1 A symmetry boundary condition is applied to the portion of the boundary ahead of the leading edge of the plate. The density contours of the flat plate are shown in Fig. 2. The edge shock and the boundary layer are appeared clearly as we expected. Fig. 3 compares profiles of skin friction distribution with Carter's numerical results[5], showing good agreement away from the leading edge. The slight discrepancy of skin friction around the leading edge is attributed to Carter's grid not being fine enough near the stagnation singularity point.

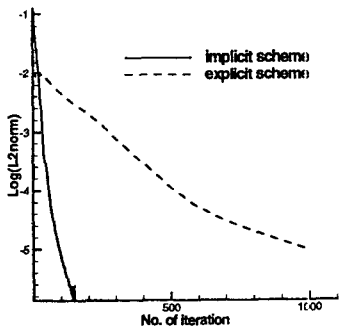

Fig. 4 Convergent history of energy variable

Convergence rates of energy variable for the fully implicit (s_1=1.0, s_2=1.0, s_3=1.0, s_4=1.0) and explicit (s_1=1.0, s_2=1.0, s_3=1.0, s_4=1.0) schemes are compared in Fig. 4. The convergence rate of implicit scheme is much more rapid than that of the explicit scheme.

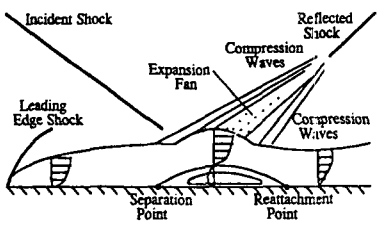

Fig. 5 Schematic representation of shock wave boundary layer interaction.

A schematic representation of shock wave boundary layer interaction is shown Fig. 5. An incident shock wave is generated by a wedge with a deflection angle θ. The incident shock impinges on a straight wall and reflects outward. A strong incident shock separates the boundary layer. The thickening of the boundary layer due to the shock impingement generates outgoing compression waves and expansion fan. The compression waves rapidly coalesce to form the reflected shock.

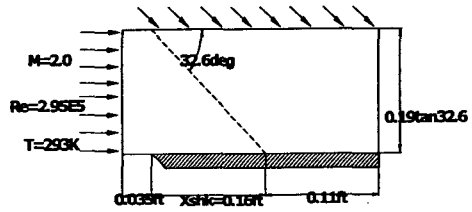

Fig. 6 Geometry and freestream conditions of Hakkinen's shock wave boundary layer interaction experiment

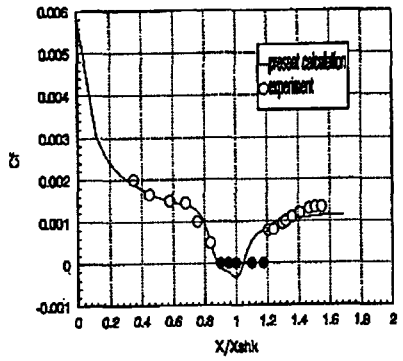

Fig.7 Comparison between the present results and Hakkinen's experimental data of the skin friction

The experiments of Hakkinen et al. [6] are employed to validate the numerical schemes as a test case. The inflow conditions of Mach number M=2.0, Reynolds number $Re_{Xshk}=2.96x10^5$, and temperature $T_\infty=293K$ are shown in Fig. 6. Incoming shock angle of 32.6° is sufficient to cause the boundary layer separation.

The distribution of the skin friction along the flat plate is compared with the experimental data of Hakkinen et al. in Fig. 7. It is noted that the experimental skin friction probes are unable to measure skin friction in the separated region other than to show that it is zero, indicated by the solid symbols where the presence of separated flow is identified.

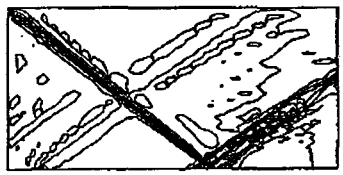

(a) Pressure contours (Max=0.2509, Min=0.01727, Δ=0.00516)

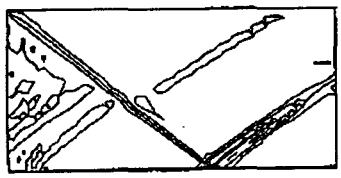

(b) Density contours (max=1.271, Min=0.6915, Δ=0.03864)

Fig. 8 Pressure and temperature contours on flat plate

Computed density and pressure contours are

shown in Fig. 8. Reflected shocks stand on the separation and reattachment points.

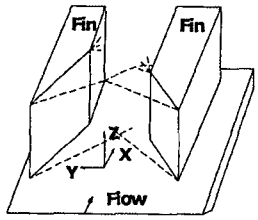

Fig. 9 Schematic representation of asymmetric crossing shock wave turbulent boundary layer interaction

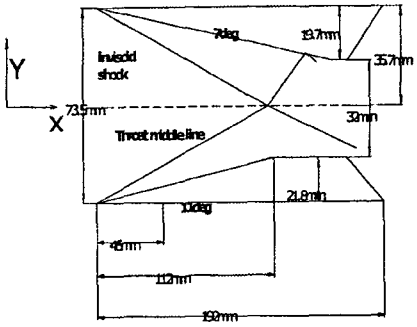

Fig.10 Sketch of asymmetric double fins with $M_\infty = 3.85, \mathrm{Re}_{\delta_\infty} = 3x10^5, P_t = 1.5\mathrm{Mpa}$, $T_t = 270\mathrm{K}, \delta_\infty = 3.5\mathrm{mm}$

More complex three-dimensional shock wave boundary layer interaction occurs on asymmetric double fins. The geometry and a sketch of asymmetric double fins experimented by Knight [7] are shown in Figs. 9 and 10.

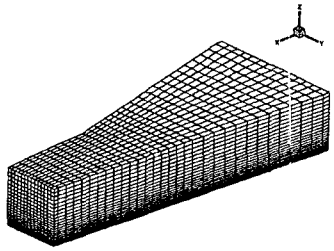

Fig. 11 Meshes of asymmetric double fins

Fine meshes are applied only to solve the boundary layers on the bottom surface. The thin boundary layers on the fin surfaces are not resolved and slip boundary conditions are employed at the fin surfaces. Previous studies[8] have demonstrated that the shock-wave/turbulent-boundary layer interaction is essentially unaffected by the boundary layer on the fin.

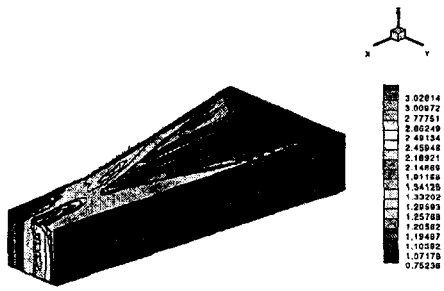

(a) Density contours

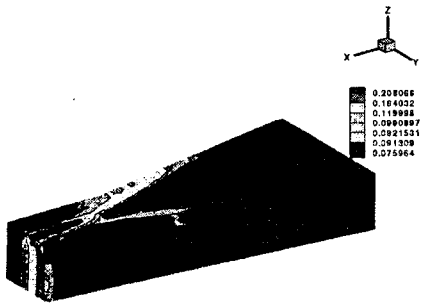

(b) Pressure contours

Fig.12 Density and pressure contours. Existence of crossing shock waves and expansion waves appear

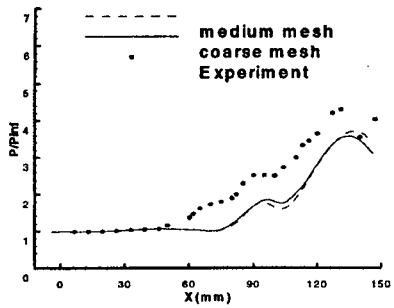

Fig. 13 Comparison between the present result and experimental data of wall pressure on the throat middle line

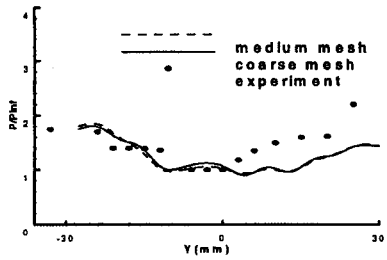

Fig. 14 Comparison of wall pressure at 46mm for the present result and experimental data

Figs. 12(a) and (b) show the contours of density and pressure, respectively. The crossing shock waves and expansion waves in the asymmetric double fins is clearly evident in the figures. The present results in the throat middle line and at streamwise location, x=46mm, are compared with experimental data for wall pressure in Fig. 13 and 14. The present study of surface pressure on the throat middle line is in agreement with the experimental data upstream but deviate toward downstream. At x=46mm, there are good agreements between the present data and experimental data.

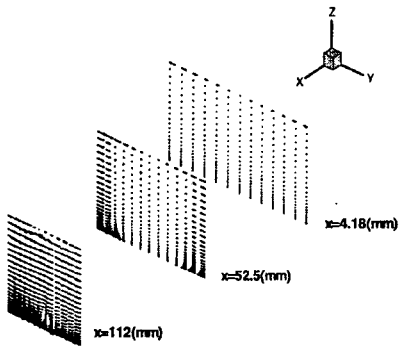

Fig. 15 Velocity vectors at different streamwise stations

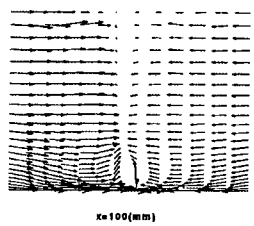

Fig. 16 Crossflow velocity vectors at x=112(mm)

Fig. 15 shows crossflow velocity vectors at different streamwise planes in the x-direction.

Velocity vectors at 112mm in the x-direction are magnified in Fig. 16. Evidently, the left and right vortices are generated due to the double fins near the surface downstream

4. Conclusions

The theory of mixed explicit-implicit generalized Galerkin finite element method is developed to analyze shock wave turbulent boundary layer interactions. Several benchmark problems have demonstrated that the proposed computational scheme is able to solve high speed compressible flows.

References

[1] Moon, S. Y., Yoon, K. T., and Chung, T. J., "Numerical simulation of heat transfer in chemically reacting shock wave turbulent boundary layer interactions", Numerical Heat Transfer. Vol. 30, No. 1, 1996, p. 55-72.

[2] Chung, T. J. and Yoon, W. S., "Hypersonic combustion with shock wave in turbulent reacting flows", AIAA paper 92-3426, 1992

[3] Sarkar, S., "Application of Reynolds stress turbulent model to the compressible shear layer", AIAA paper 91-0523, 1991

[4] Moon, S. .Y. " Applications of FDMEI to chemically reacting shock wave boundary layer interactions", Ph. D. dissertation,UAH press, 1998

[5] Carter, J. E., "Numerical solutions of the Navier-Stokes equations for the supersonic laminar flow over a two-dimensional compression corner", NASA Technical Report R-385, 1972.

[6] Hakkine, R. J., Greber, I., Trilling, L., and Abarbanel, S. S., "The interaction of an oblique shock wave with a laminar boundary layer", NASA Memorandom218-59w, March 1959.

[7] Knight, D. D., Garrison, T. J., Settles, G. S., Zheltovodov, A. A., Maksimov, A. I., Shevchenko, A. M., and Vorontsov, S. S., "Asymmetric crossing-shockwave/turbulent-boundary-layer interaction", AIAA Journal, Vol. 33, No.12, 1995, p.2241-2249

[8] Knight, D., Badekas, D., Horstman, C., and Settles, G., "Quasi-conical flowfield structure of the three-dimensional single fin interaction", AIAA Journal, Vol. 30., No. 12, 1992, p.2809-2816.